Journal of Sol-Gel Science and Technology
https://doi.org/10.1007/s10971-025-06898-z

ORIGINAL PAPER

Synthesis and characterization of undoped and yttrium-doped zinc oxide thin films by sol–gel spin coating method

Rahik Ibne Forman[1] · Md. Al-Riad Tonmoy[1] · Maruf Ahmed[1] · S. M. Nasim Rokon[1,2]

Received: 7 February 2025 / Accepted: 2 August 2025

Abstract

This work demonstrates the deposition of n-type zinc oxide (ZnO) and Yttrium (Y) doped ZnO (Y-ZnO) thin films on quartz glass substrates with the variation of the concentration of Y at different percentages (1, 3, and 5 at. %) as the dopant. ZnO and Y-ZnO films were successfully deposited using the sol–gel spin coating method and subsequently annealed at 500 °C. Deposited thin films exhibited well-defined polycrystalline structures with a hexagonal wurtzite crystal configuration. Y doping effect in ZnO thin film was investigated from of structural, morphological, and optical analysis. Synthesized thin films were characterized by means of X-ray diffraction (XRD), Scanning Electron Microscopy (SEM), Electron Dispersive Spectroscopy (EDS), and Ultraviolet-visible (UV-vis) spectroscopy. XRD patterns indicated the decreased crystallinity in 1% Y doping with some impurity content and less intense peaks compared to undoped ZnO. However, this drawback was improved significantly in case of 3% and 5% Y doping due to the successful substitution of Zn^{2+} site by Y^{3+} ion in ZnO lattice. As dopant concentration increased, the increment trend of crystallite size (from 2.16 to 8.87 nm) was also observed. SEM examination demonstrated Y's domination over ZnO thin film morphology. The particles mostly showed agglomeration and irregular forms, with an average size ranging from 44.96 nm to 27.24 nm. The EDS spectrum confirmed the presence of Zn, O, and Y elements. Additionally, all the synthesized thin films demonstrated high transparency in the visible range, with values ranging from 81.54% to 89.83%. Because of the dopant element's dispersion, the high transparency that was seen in the undoped ZnO thin film dropped to 87.7% in the 5% Y doping. The bandgap was reduced from 3.22 to 3.06 eV with the increment of the dopant concentration due to the quantum confinement effect.

Graphical Abstract

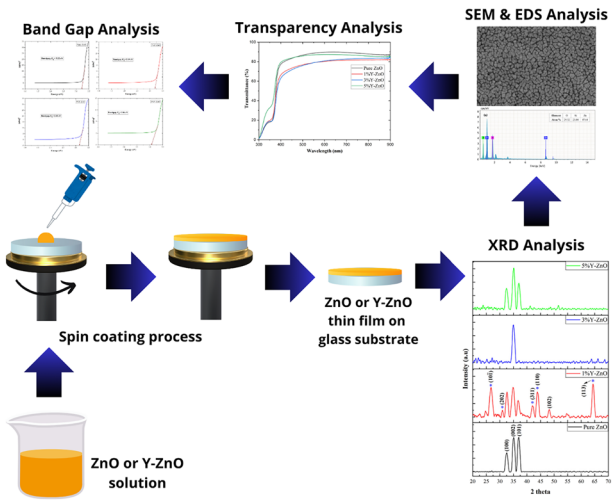

✉ S. M. Nasim Rokon
rokon@mse.ruet.ac.bd

[1] Department of Materials Science & Engineering, Rajshahi University of Engineering & Technology, Rajshahi, Bangladesh

[2] Department of Materials and Metallurgical Engineering, Bangladesh University of Engineering and Technology, Dhaka, Bangladesh

Published online: 13 August 2025

Keywords Yttrium-doped zinc oxide · Thin film · Sol–gel deposition · Spin coating · Structural properties · Optical properties

Highlights

- Undoped and Yttrium (1, 3, and 5 at. %) doped ZnO thin films were successfully synthesized through the sol–gel spin coating method where all films exhibited a polycrystalline hexagonal wurtzite structure.
- Along with Zn and O components, Y was proven to be present in the ZnO matrix by EDS, whereas SEM showed uneven and agglomerated particles.
- In the visible range, optical transparency remained high, but the quantum confinement effect caused the optical bandgap to follow a decreasing trend.

1 Introduction

A thin film is a layer of material that is 10 nm to 1-2-μm thick and is applied to a substrate using physical or chemical techniques. This process is called thin-film technology. These films are classified as dielectric, metallic, organic, or semiconductor based on composition [1]. A well-researched II-VI semiconductor, zinc oxide (ZnO) holds significance due to its distinctive characteristics and wide range of applications. ZnO exhibits excellent transparent optical qualities in the visible spectrum, a large direct band gap of 3.37 eV, and a significant excitonic binding energy of 60 meV [2–4]. It also displays UV absorption, chemical stability, and significant surface-sensitive catalytic activity [5–7]. ZnO thin films are crucial in optoelectronic applications, including thin-film transistors, photocatalysts, gas sensors, UV light emitters, and solar cells, due to these key features [3, 8, 9]. Recent advances in nanofabrication have further enhanced the quality of ZnO nanostructures, which are non-toxic, antibacterial, and easy to fabricate. The combination of high transmittance, thermal stability, and versatility highlights ZnO thin films as a promising material for cutting-edge technologies [6, 10, 11].

In recent years, doping ZnO thin films with rare earth elements such as lanthanum (La), scandium (Sc), and yttrium (Y) has gained significant attention. These dopants help reduce native point defect densities in ZnO, thereby improving its structural, optical, and morphological properties [3, 12]. Again, they are particularly attractive due to their non-toxicity, natural abundance, and ability to introduce intra-4f optical transitions. Particularly, Yttrium (Y) doped ZnO (Y-ZnO) thin film is highly valued for its enhanced optical, electrical, and structural properties. Y stands out among dopants due to its ionic radius, which closely matches that of Zn, allowing it to replace Zn^{2+} in the lattice [7, 13–15]. This substitution introduces free electrons, improving electrical conductivity and optical transmittance [16, 17]. On the other hand, the strong Y-O bond (719.6 kJ/mol) minimizes oxygen vacancies, enhancing stability and reducing defects. Y-ZnO thin films exhibit improved UV emission, photocatalytic performance, and suitability for transparent conducting coatings, making them ideal for applications like UV emitters, sensors, and transparent electrodes [16–18].

There are several ways to develop ZnO thin films, including basic erosion, ink-jet printing, sol–gel, spray pyrolysis, physical vapor deposition (PVD), chemical vapor deposition (CVD), sputtering, and pulsed laser deposition (PLD) [3, 8, 10, 11, 19]. The sol–gel method is a preferred technique for fabricating thin films, particularly ZnO and Y-ZnO, due to its cost-effectiveness and versatility. It offers excellent control over chemical composition, allowing precise adjustments to material properties [15, 19, 20]. The process is simple, low-cost, and uses low annealing temperatures, making it suitable for large-scale production. Additionally, it ensures high purity, homogeneity, and control over film composition and size. Compared to other synthesis methods, sol–gel is particularly advantageous for producing high-quality YZO films with uniform properties and low process temperatures [10–12]. By eliminating the requirement for time-consuming vapor phase equipment, the sol–gel spin coating technology provides a direct deposition method with high throughput. A number of deposition parameters, including spin speed, precursor concentration, and pre- and post-heating techniques, affect the characteristics of ZnO thin films produced by spin coating. Notably, post-heating treatment holds particular significance as it significantly impacts crystalline structure and surface texture adjustments [5, 6, 21].

In previous studies, Y-ZnO nanostructured thin films have been reported with different amounts of Y addition [7, 10, 14, 16]. For example, Ivanova et al. [7] examined the structural and optical behavior of undoped and Y-ZnO thin film that were fabricated by the sol–gel spin coating technique. In contrast to the undoped films, the XRD analysis showed structural and phase changes in the doped films as well as a downward trend in the bandgap values [7]. Similarly, Y-ZnO thin films with a polycrystalline hexagonal wurtzite structure were obtained by Bashir et al. [13] applying the spin coating method to glass surfaces. At a 2 at

% Y doping level, the films displayed 88% transmittance in the visible spectrum with 3.23 eV bandgap energy [13]. Utilizing sol–gel spin coating technique, Thirumoorthi et al. [3] produced apparent conducting Y-ZnO thin films where XRD examination verified hexagonal wurtzite phase and a polycrystalline structure. Y doping caused the optical bandgap to blue shift and increased the optical transmission (78–83%) in the visible spectrum [3]. Ghanem et al. [22] used the sol–gel spin coating method to fabricate undoped and erbium (Er)-doped ZnO thin films. As the rate earth element, Er concentration increased from 0.0 to 1.5 mole%, an enhancement in crystallinity and reduced bandgap energy (from 3.24 eV to 2.95 eV) were found [22]. By using the same technique, incorporation of Europium (Eu) in concentrations of 0.4, 0.6, 0.8, and 1 mol% into a ZnO thin film, Hasabeldaim et al. [23] observed a deterioration in film crystallinity. As a result, the bandgap somewhat decreased and average transparency of about 80% in the visible spectrum [23]. Sharma et al. [24] doped ZnO thin films with Scandium (Sc), a rare-earth and group III element, on glass substrate. When the temperature of annealing was raised to 400 °C, the films showed a discernible rise in peak intensity and a preferential (002) alignment along the c-axis [24]. This study is the systematic analysis of structural and optical variations in sol–gel spin-coated Y-doped ZnO thin films with low to high Y doping concentrations (1%, 3%, and 5% at. %) on quartz substrates to provide a summary of the activity of Y as a dopant in ZnO thin films which isn't done yet as per authors' knowledge.

This work aims to fabricate extremely transparent (89.83%) undoped ZnO and Y-ZnO thin films on quartz glass substrates using the cost-effective and useful sol–gel spin coating technique. The sols had varying yttrium precursor concentrations and a much lower to higher concentration of doping element (Y: 1, 3, and 5 at. %). The objective was to investigate the changes of structural, morphological and optical properties of thin films after annealing at 500 °C. All the thin films demonstrated a polycrystalline nature, characterized by a hexagonal wurtzite crystal structure. The structural attributes, surface morphology, and optical features of the thin films made on quartz glass substrates were examined in connection to the dopant concentration.

2 Materials

Zinc acetate dehydrate (ZAD) [$(CH_3COO)_2Zn.2H_2O$, 98%] as starting material, 2-methoxyethanol ($C_3H_8O_2$, 99%) as solvent, and Monoethanolamine (MEA) (C_2H_7NO, 99%) as stabilizer were purchased from Research Lab Fine Chem Industries, India. Yttrium (III) Nitrate Hexahydrate (YNH) [$Y(NO_3)_3.6H_2O$], assay 99.9%, as doping material was from Sisco Research Laboratories Pvt. Ltd., India. Ethanol (CH_3CH_2OH, ≥99%, Merck), Acetone (CH_3COCH_3, ≥99.8%, Merck), and Deionized water were also used for performing this whole work.

2.1 Experimental method

The sol–gel spin coating method was used to fabricate the undoped and Y-ZnO thin films on quartz glass substrates at room temperature. A flowchart and an overview of the process that is used for producing highly transparent Y-ZnO thin films are shown in Fig. 1. At room temperature, 0.4 M ZAD and YNH were dissolved in a 2-methoxyethanol solvent to prepare the sol. The concentration of Y was changed in increments of 1%, 3%, and 5% by using YNH as a dopant. When the sol for the undoped ZnO thin film was being prepared, no dopant was added. MEA was progressively added dropwise to the solution in an equimolar ratio (ZAD: MEA = 1:1) in order to eliminate precipitates and turbidity. Using a magnetic stirrer, the resultant mixture was constantly swirled for two hours at 80 °C and 400 rpm. For the solution to reach the required viscosity, it was then aged for a full day. The surface of glass substrates was cleaned with detergents and washed with water before thin film deposition. Next, it was ultrasonically cleaned for five minutes in DI, ethanol, acetone, and DI. Clean quartz glass substrates were spin-coated with the prepared solution for 10 s at 1000 rpm and then for 20 s at 3000 rpm. Coated substrates were dried for five minutes at 200 °C on a hot plate to get rid of organic residues. For two hours, the thin films that were deposited were annealed at 500 °C.

2.2 Characterization of thin films

A Shimadzu LabX XRD-6100 diffractometer was used for XRD analysis in order to describe the thin films' structural characteristics. Surface morphology was analyzed with a ZEISS Sigma 360 SEM and for the elemental analysis or EDS Sigma 560 was used. Using a Shimadzu UV-3600 Plus UV-VIS with NIR spectrometer, the optical characteristics were assessed.

3 Result and discussion

3.1 Structural properties

The X-ray Diffraction (XRD) patterns of the undoped and Y-ZnO thin films are presented in Fig. 2a. The XRD peaks appeared mainly at diffraction angles of 32.58°, 35.1°, and 36.96° correspond to (100), (002) and (101) planes, respectively [Reference code: 96-230-0117]. XRD analysis of all the thin films reveals a polycrystalline structure

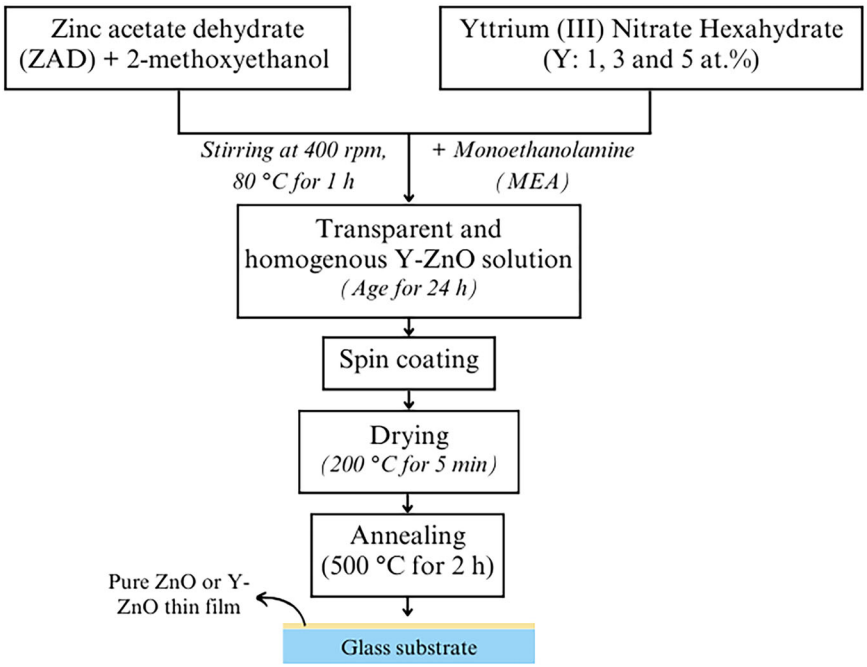

Fig. 1 Flow chart for the synthesis of Y-ZnO thin film via sol–gel process.

featuring a hexagonal wurtzite crystal configuration with a space group of $P6_3mc$. The undoped ZnO film exhibits crystallites that are primarily oriented with the (002) and (101) planes parallel to the substrate surface, along with the (100) reflection. This indicates that the orientation is favored kinetically, which consequently highlights that the greatest concentration of Zn atoms is located along these planes [11, 25].

The intensity of the (002) diffraction peak decreases in 1% Y-ZnO thin film but then progressively increases as the dopant concentration rises. This trend can be attributed to enhanced crystallinity in 3% and 5% Y-ZnO thin films, resulting from the creation of additional nucleation centers facilitated by the dopant atoms [10, 26, 27]. The crystallinity of the thin films were calculated by using the following equation [28, 29]:

$$Crystallinity(\%) = \frac{Area\ of\ crystalline\ domain(S_c)}{Total\ area(S_c + S_a)}$$

Where S_a represents the area of amorphous region. The crystallinity of 1% Y-ZnO thin film is decreased compared to undoped thin film sample. Y doping inhibits the crystallization of the film, as clearly observed in the 1% Y-ZnO thin film. Moreover, small amount of impurities appeared in the XRD spectra resulting in extra peaks at $2\theta = 26.75°$, 30.95°, 42.08°, 43.76°, and 64.33° (marked with blue asterisk) which is another prominent reason for decreased crystallinity. Among them, 26.75° and 64.33° can be assigned to silica (SiO_2) [Reference code: 96-153-2513] and the peak at 42.08° can be assigned as Cristobalite [Reference code: 96-901-7506] which is another form of SiO_2. Furthermore, peak at 30.95° can be mentioned as the SiO_2 zeolite [Reference code: 96-411-2883]. The peak at 43.76° can be denoted as Yttrium Zinc Silicide [Reference code: 96-152-7634]. Conversely, no additional phases are detected in 3% Y-ZnO and 5% Y-ZnO thin film, indicating high phase homogeneity. This suggests that Zn^{2+} sites in the ZnO lattice are substituted by Y^{3+} [26, 30].

While the (100) and (101) planes are invisible in 3%Y-ZnO thin films, the (002) plane has a favored orientation because it is kinetically preferred. The nanostructure of this thin film demonstrated a high degree of c-axis orientation, which is reliant on the surface and interfacial energies of the film and the glass substrate. Slower growing planes have the lowest surface energy and so fast-growing planes in crystal development tends to disappear [11, 31]. As a result, the ZnO thin film's (001) and (101) planes vanish during development, and the direction of growth is perpendicular to the glass substrate along the (002) plane with the maximum density of Zn atoms [11]. The absence of precursor-related signals are absent in 3% and 5% Y-ZnO thin film can be attributed to the effective dopant incorporation and high degree of c-axis orientation which reduces the formation of any secondary phases [13, 32]. Peak position shifts as a result of the increased space between crystal planes resulting from Y^{3+} substituting Zn^{2+} in the ZnO crystal lattice. Unlike the undoped ZnO thin film, the doped ZnO thin film's (002) peak position changes to lower diffraction angle as the Y^{3+} concentration rises [Fig. 2(b)]. This is likely because Y^{3+} replaces Zn^{2+}, causing some tensile lattice strain. However, because of appropriate substitution, no strain is seen in the 5% Y-ZnO thin film [3, 12].

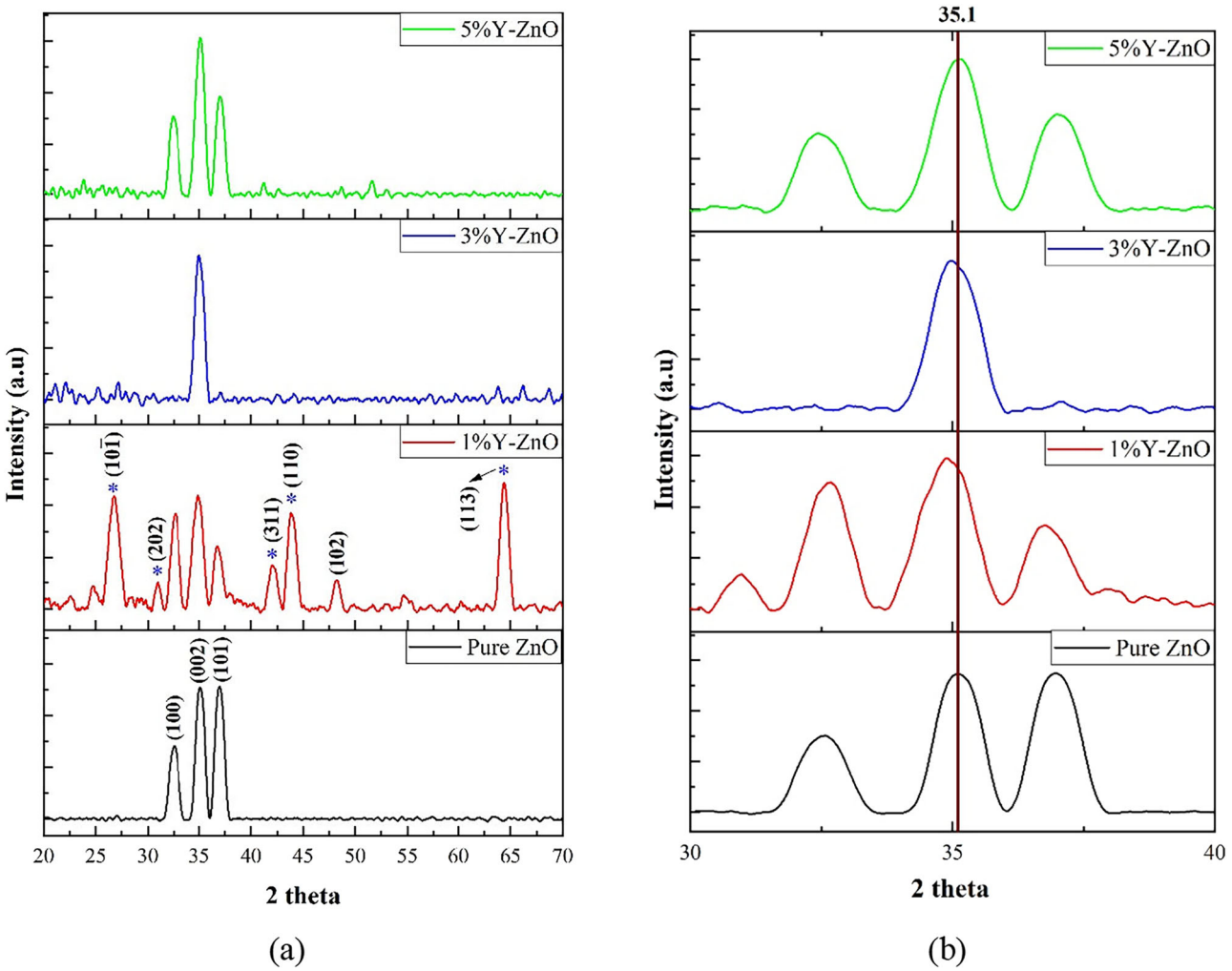

Fig. 2 **a** XRD curves of the undoped, 1%, 3%, and 5% Y dopped ZnO thin films, and **b** peak shifting behavior because of Y doping in ZnO thin film.

Table 1 Calculated crystallite size (D), interplanar spacing (d), crystallinity, dislocation density, and micro-strain from XRD data of the undoped, 1%, 3%, and 5% Y-doped ZnO thin films.

Sample	FWHM, β (degree)	Crystallite size, D (nm)	Interplanar spacing, d (Å)	c (Å)	Crystallinity (%)	Dislocation density, $\delta \times 10^{-3}$ (nm^{-2})	Micro strain, $\varepsilon \times 10^{-3}$
Undoped ZnO	3.86	2.16	2.55	5.11	214.37	98.47	53.23
1%Y-ZnO	3.54	2.35	2.57	5.14	181.15	18.71	49.21
3%Y-ZnO	0.95	8.78	2.56	5.13	12.96	44.85	13.13
5%Y-ZnO	0.94	8.87	2.55	5.11	12.70	76.67	12.95

The thin film samples' different structural properties, as determined by the XRD data, are presented in Table 1. The average crystallite size (D) of thin films is calculated using the full width at half maximum (FWHM) of the (002) diffraction peak, applying the Debye-Scherrer formula [16, 30]:

$$D = \frac{0.9\lambda}{\beta \cos\theta}$$

Here, λ represents the X-ray wavelength (0.154 nm), β denotes the FWHM, and θ is the Bragg angle of the diffraction peak. Because of strong surface interactions that improve the elements' mobility, the thin films' crystallite size grows from 2.16 to 8.87 nm. As atoms gain sufficient energy during annealing, they migrate and rearrange into thin films [3, 10]. Though increment of crystallite size is observed along with the addition of dopant element, the crystallinity decreases. This

behavior can be attributed to the lattice distortions and introduction of defects due to ionic size difference between the Y^{3+} and Zn^{2+}. When localized crystalline domains get larger, these defects affect general crystallinity by interfering with crystallite alignment and disrupting long-range ordering in the crystal structure [13, 17, 30].

By using the Bragg equation interplanar spacing (d) values are determined [27]:

$$2d \sin\theta = n\lambda$$

The Zn^{2+} and Y^{3+} ions have distinct oxidation states and respective radii of 0.088 and 0.104 nm. Substituting an atom with a larger one would increase the d value which is observed in 1% and 3% Y-ZnO thin film. Conversely, the opposite effect is observed due to the higher oxidation state of the substituting atom in the 5% Y-ZnO thin film. Proper doping can be a reason for having the same d value as undoped ZnO thin film [30].

Lattice parameters are determined along the c-axis from the formula [14]:

$$\left(\frac{1}{d_{hkl}}\right)^2 = \frac{4}{3}\left(\frac{h^2 + k^2 + hk}{a^2}\right) + \left(\frac{l^2}{c^2}\right)$$

The thin films' c-axis lattice parameters rise from 5.11 to 5.13 Å as the Y^{3+} content increases. This increase remains steady for the 5% Y-ZnO thin film compared to the undoped one. The reason behind this is the larger size of Y^{3+} compared to Zn^{2+} and substitution into the lattice or interstitial sites of ZnO. In the 5% Y-ZnO thin film, the c-axis lattice constant remains the same as the undoped ZnO thin film. This may suggest the saturation of dopant incorporation introducing compressive strain. This compressive strain tackles the initial expansion of substitution of Zn^{2+} by Y^{3+}. When compressive strain fully counteracts the substitutional expansion, the system obtains equilibrium [33]. This consistent behavior aligns with the absence of peak shifting, indicating no strain [26].

The dislocation density (δ) and the micro-strain (ε) in the deposited films are calculated as [30]:

$$\delta = 1/D^2$$

$$\varepsilon = \beta/(4\tan\theta)$$

Increasing doping concentration (3% and 5%) leads to a noticeable decrease in ε on the (002) plane, indicating stress release in the films. This suggests that Y^{3+} doping boosts film crystallization and improves structural integrity by boosting D and decreasing micro-strain. However, in 1% Y-ZnO thin film, existence of secondary phases increases micro-strain and dislocation density compared to 3% and 5% Y-ZnO thin films.

3.2 Surface morphology

Scanning Electron Microscopy (SEM) analysis was conducted to evaluate the surface morphology of undoped and Y-ZnO thin films presented in Fig. 3a–d. The particles were irregular in shape and exhibited agglomeration. The ZnO thin films' surface morphology was significantly affected by the Y^{3+} doping concentration. The undoped thin film sample (Fig. 3a) showed a porous nanostructure composed of irregularly shaped particles on the substrate. For the 1% Y-ZnO thin film (Fig. 2b), cracks are observed which is directly correlated with the XRD analysis. This may be because of stress generation caused by the size difference between Zn and Y ions. Some extra peaks were present in XRD as impurities and this can be a reason for the formation of cracks and irregular texture in this sample. For the 3% and 5% Y-ZnO thin film (Fig. 3c, d), more compacted nanostructure and texture is observed which denotes the improved crystallinity which correlates with the XRD data.

Figure 4 displays the particle size distribution, which were measured using ImageJ software. A comparison of undoped, 1%, 3%, and 5% Y-ZnO revealed that the average particle sizes were 44.96 nm, 39.01 nm, 30.77 nm, and 27.24 nm, respectively. Several factors may contribute to the decrease in particle size with increasing doping concentration. An increased dopant concentration can lead to the generation of various defects, primarily influenced by the mobility of interfaces and the accelerated growth of nanocrystalline domains. As seen in Table 1, the dislocation density determined by XRD correlates with the reduction in particle size in the thin film samples. The increase in Y^{3+} percentage enhances the packing density of the dopant, resulting in closely packed ZnO lattice and a decrease in particle size. Y^{3+} ions may act as nucleation sites, leading to a greater number of smaller particles as the material is distributed among more nuclei. This nucleation process limits the growth space for the host lattice [15, 17]. Both the host and dopant crystallite borders limit crystallite growth, which might impede the development of crystals and ultimately result in smaller-sized particles [34]. Nevertheless, it is discovered that the particle size seen by SEM examination is larger than the crystallite size determined by XRD peak profile analysis. The particle size obtained from SEM includes crystalline aggregates, meaning the particles are not monocrystalline. Additionally, anisotropy in particle shape could contribute to this difference, as SEM measurements are taken along the plane of the film surface, while XRD determines the size by considering multiple directions [16, 27].

Energy Dispersive X-ray Spectroscopy (EDS) spectra were used to examine the chemical compositions in weight percentage of all thin films. The EDS spectra of undoped and Y-ZnO thin films are shown in Fig. 5a–d. The XRD graph also reveals that the maximum concentration of

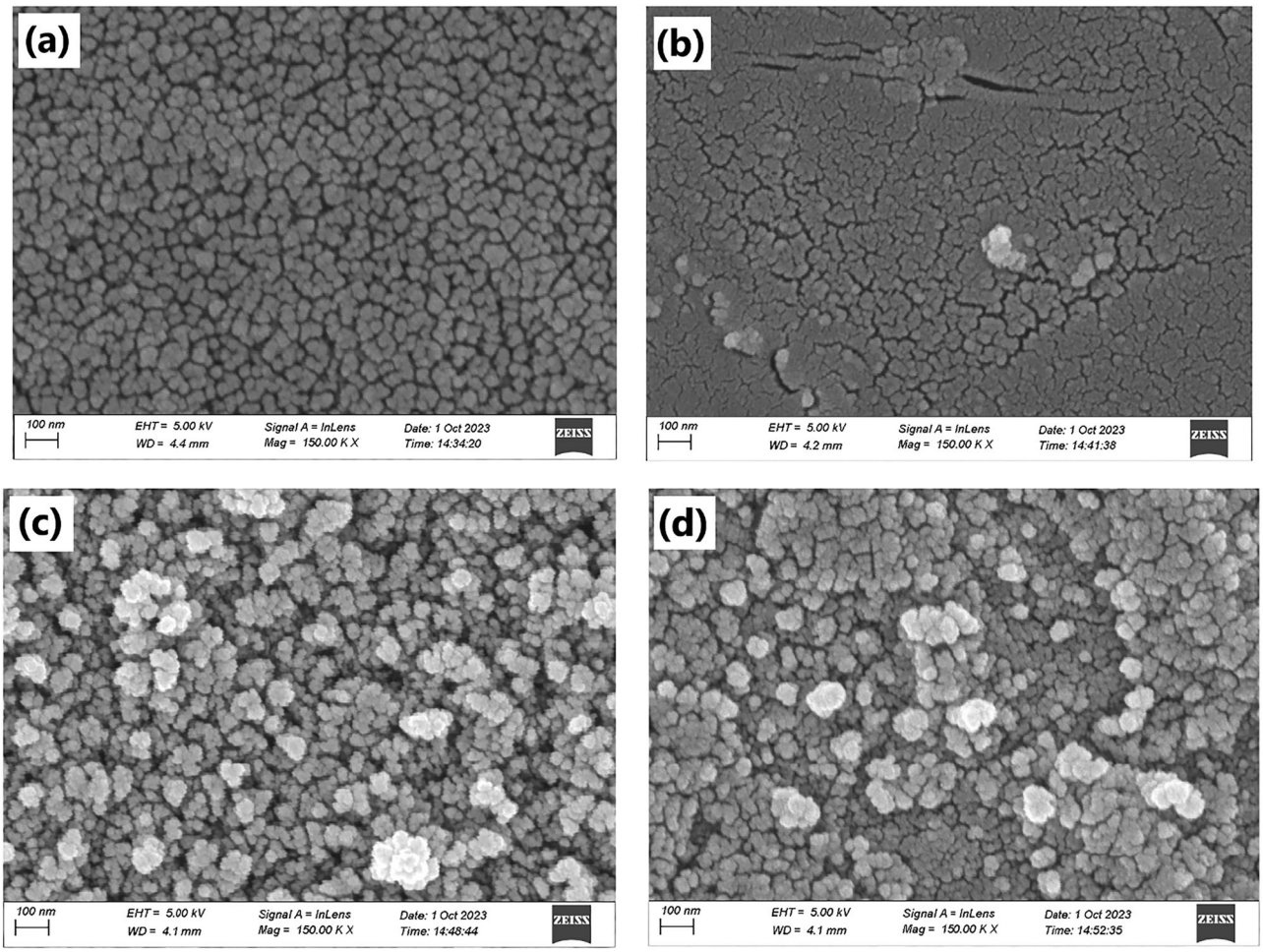

Fig. 3 SEM micrographs of the **a** undoped, **b** 1%, **c** 3%, and **d** 5% Y-doped ZnO thin films.

silicon (Si) is found in the 1% Y-ZnO thin film. Higher porosity from dopant-induced structural modifications and thinner films as a result of changed growth kinetics may arise from increased Y doping concentrations. Both of these aspects allow measurement beams to penetrate the substrate more deeply, facilitating Si detection and increased Si content in higher Y-doped ZnO thin films [35, 36]. The graph of the Y-ZnO thin film samples shows obvious peaks for Y in addition to Zn and O peaks, indicating that Y was incorporated into the doped ZnO samples. This again confirms that Y^{3+} ions have effectively replaced Zn^{2+} in the hexagonal crystal lattice, aligning with the results of the XRD analysis [34].

3.3 Optical properties

The optical properties of the thin films were analyzed using UV-Vis spectroscopy. Figure 6a displays the spectra of transmittance of deposited thin films. The spectra show very high transmittance across the visible spectrum, ranging from approximately 81% to 89%. Specifically, the transmittance of the undoped ZnO thin film in the visible range is approximately 89%. But after adding 1% Y, 1% Y-ZnO thin film shows lower transmittance in comparison to undoped ones which is around 81%. This behavior can be attributed to the introduction of structural defects. Absorption from these defect-related states increases resulting the decrease of transmittance [13, 33]. On the other hand, an increasing trend of transmittance is observed in 3% Y-ZnO and 5% Y-ZnO thin films indicating compensation of defects and oxygen vacancies which works as light absorption centers [37]. Again, from Table 1 the increment of crystallite size is observed. This behavior and improved grain boundary structure reduces the light scattering resulting the increment of transmittance than the 1% Y-ZnO thin film [38].

The synthesized thin film samples' absorbance spectra are shown in Fig. 6b. Absorption edge shifting towards either lower or higher wavelengths suggests a corresponding decrease or increase in the bandgap of thin films [14]. The optical bandgap of undoped and Y-ZnO films is determined from the absorption spectra using the following equation, which relates the absorption coefficient (α) to the optical bandgap (Eg), based on the Tauc model [27]:

$$(\alpha h\nu)^2 = A\left(h\nu - E_g\right)$$

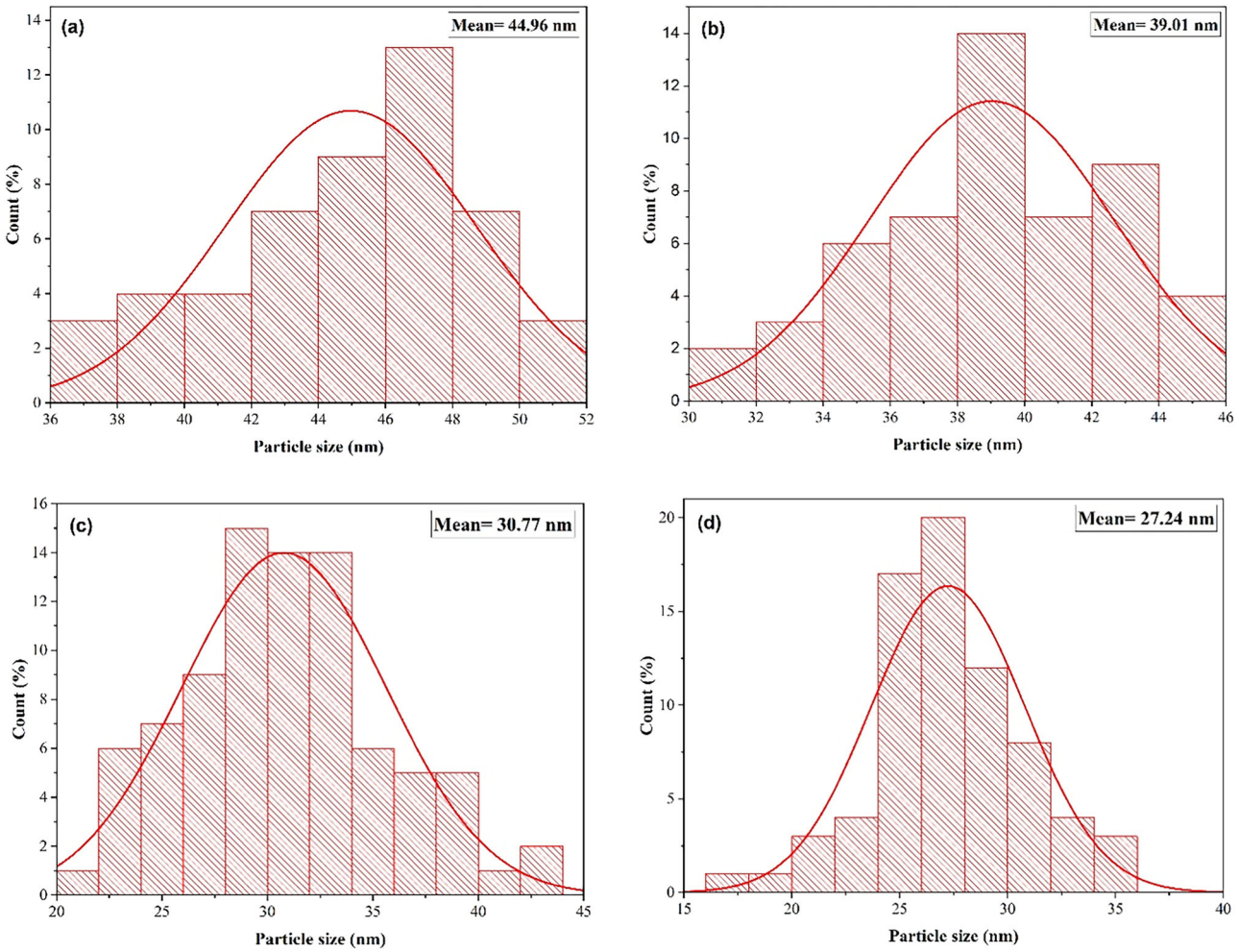

Fig. 4 Particle size distribution of the **a** undoped, **b** 1%, **c** 3%, and **d** 5% Y-doped ZnO thin films.

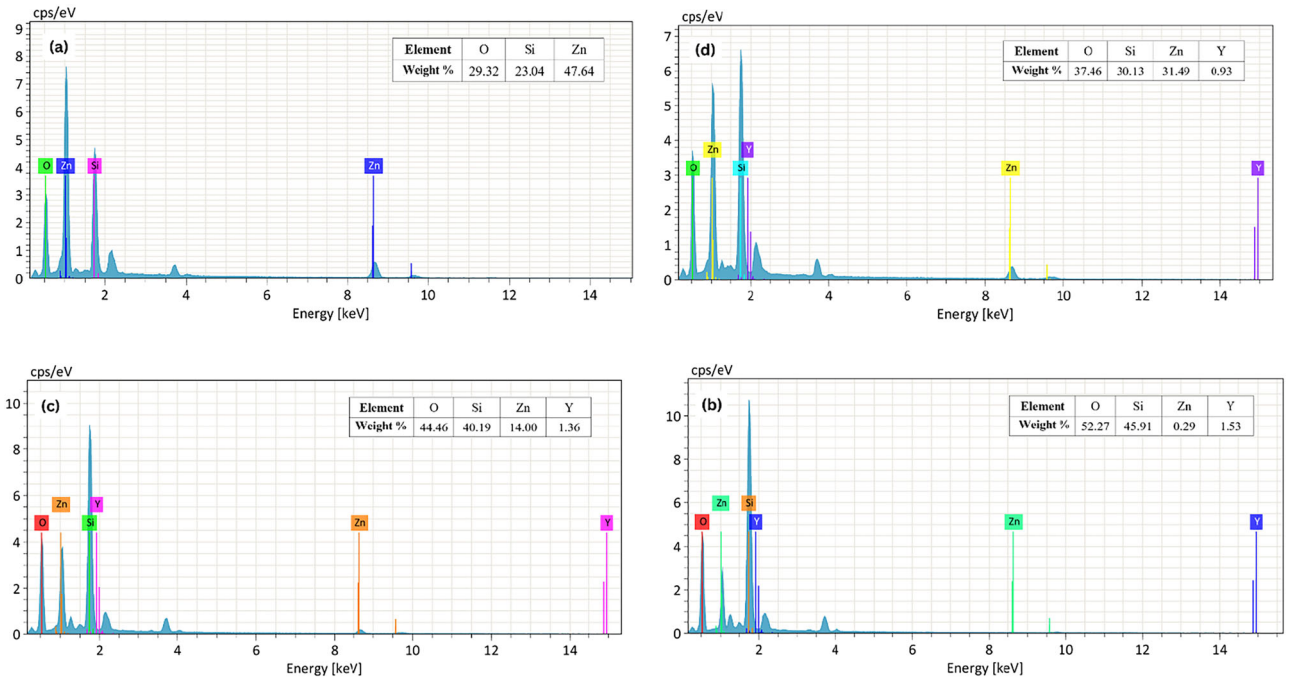

Fig. 5 EDS graph of the **a** undoped, **b** 1%, **c** 3%, and **d** 5% Y-doped ZnO thin films.

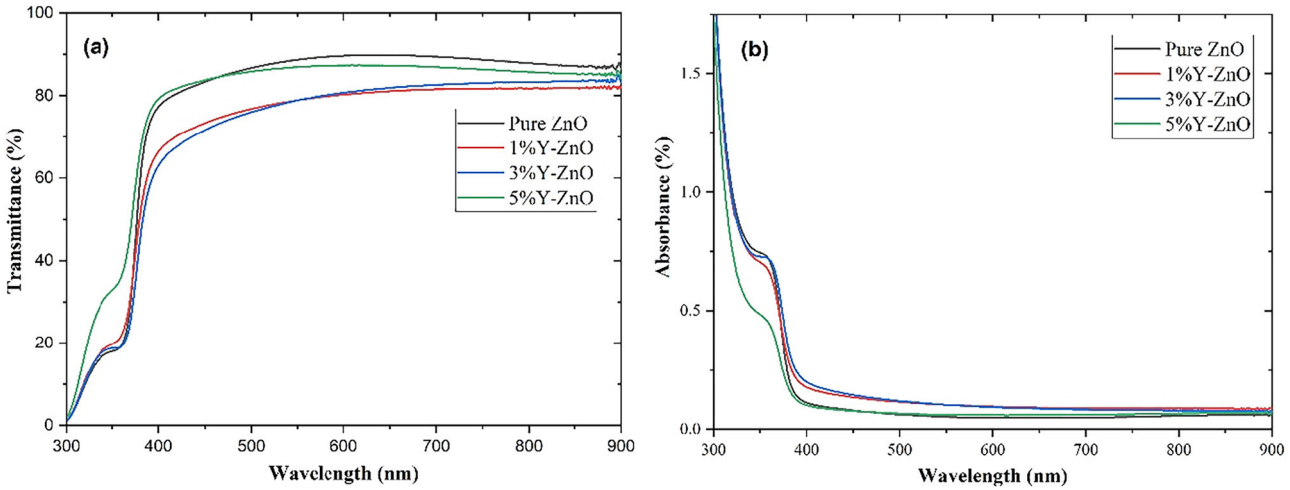

Fig. 6 **a** Transmittance and **b** absorbance spectra of all thin films.

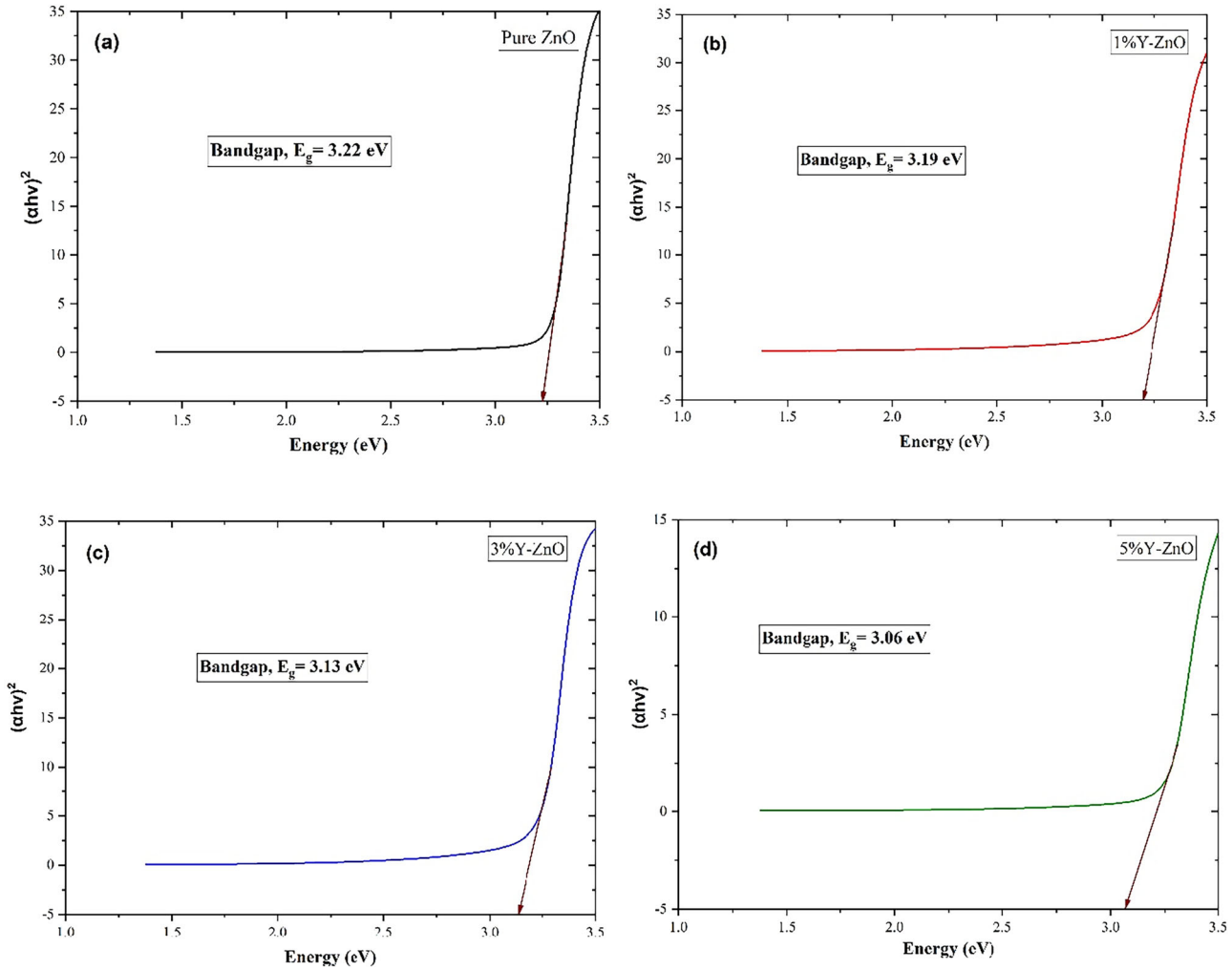

Fig. 7 Plot of $(\alpha hv)^2$ versus incident photon energy (hv) for the **a** undoped, **b** 1%, **c** 3%, and **d** 5% Y-doped ZnO thin films.

In the equation, A represents the proportionality constant and hν denotes the photon energy. From the plot of $(\alpha h\nu)^2$ against hν direct optical bandgap is calculated, as showed in Fig. 7. To get the direct bandgap of all thin films, the linear portion of the curve is extrapolated to the hν axis (x-axis). The bandgap of the undoped ZnO thin film is found to be

3.22 eV. As the doping concentration increases, this decreases to 3.06 eV at 5% Y doping. This outcome is consistent with the quantum confinement effect, which states that a decrease in the bandgap is caused by a rise in crystallite size (Table 1) brought on by a higher doping concentration. The bandgap narrows when dopant impurities are present because they cause the creation of new recombination structures having lower emission energy [7, 10].

4 Conclusion

The sol–gel spin coating method has proven to be highly effective for producing nanocrystalline thin films, as well as for depositing both undoped and Y-ZnO thin films. All films exhibited well-defined polycrystalline structure with a hexagonal wurtzite crystal configuration after annealing at 500 °C. In the XRD data, some extra peaks due to impurities were observed in 1% Y doping, which was fully recovered in the 3% and 5% Y doping in ZnO thin film. The average crystallite sizes, crystallinity, dislocation density, interplanar spacing, and micro-strains in the films were calculated from the XRD data. The synthesized thin film samples' particle size, distribution, and presence of each element were all revealed by SEM and EDS analysis. The XRD data showed good agreement with these results. The optical bandgaps for 0%, 1%, 3%, and 5% Y doping were found to be 3.22 eV, 3.19 eV, 3.13 eV, and 3.06 eV, respectively, based on the absorption spectra of the produced thin films. This effect was observed due to the quantum confinement effect. Again, decreased transparency was exhibited by 1% doping than the undoped ZnO thin film due to impurity content, but it was improved by 5% Y doping because of proper doping. 5% Y-ZnO thin film exhibited the highest transparency among the doped thin film samples but less than the undoped ones which was attributed to the scattering of light by the dopant. Thus, incorporating Y into ZnO thin films enhances their structural, morphological, and optical properties, offering new opportunities for developing stable optoelectronic devices.

Data availability

No datasets were generated or analyzed during the current study.

Acknowledgements The authors would like to thank the Department of Electrical and Electronic Engineering, Rajshahi University of Engineering and Technology (RUET), and Genome Center, Jashore University of Science and Technology (JUST), for assisting with characterization facilities.

Author contributions RIF: Conceptualization, Methodology, Investigation, Formal Analysis. MART: Formal Analysis, Writing – original draft, Writing - review & editing. MA: Conceptualization, Methodology, Investigation. SMNR: Conceptualization, Methodology, Formal Analysis, Writing - review & editing, Resources, Supervision.

Compliance with ethical standards

Conflict of interest The authors declare no competing interests.

References

1. Vyas S (2020) A short review on properties and applications of zinc oxide based thin films and devices: ZnO as a promising material for applications in electronics, optoelectronics, biomedical and sensors. Johnson Matthey Public Limited Company. https://doi.org/10.1595/205651320X15694993568524.
2. Bruno Chandrasekar L, Nagarajan S, Karunakaran M, Daniel Thangadurai T (2019) Structural, optical and electrical properties of undoped and doped ZnO thin films. In 2D Materials, IntechOpen, https://doi.org/10.5772/intechopen.88905.
3. Thirumoorthi M, Thomas Joseph Prakash J (2015) Structural, morphological characteristics and optical properties of Y doped ZnO thin films by sol–gel spin coating method. Superlattices Microstruct 85:237–247. https://doi.org/10.1016/j.spmi.2015.05.005.
4. Ahmed AS, Ahsanul Habib AKM, Shukra IJ, Alam S, Sharif A, Nasim Rokon SM (2025) Compositionally complex zinc oxide (CuxCoxMnxMgxNix)Zn1-5xO thin films synthesized by spin coating technique with enhanced band gap and transparency. J Solgel Sci Technol 113(2):450–460. https://doi.org/10.1007/s10971-024-06629-w.
5. Dahnoun M, Attaf A, Saidi H, Yahia A, Khelifi C (2017) Structural, optical and electrical properties of zinc oxide thin films deposited by sol-gel spin coating technique. Optik 134:53–59. https://doi.org/10.1016/j.ijleo.2017.01.014.
6. Mursal, Irhamni, Bukhari, Jalil Z (2018) Structural and optical properties of zinc oxide (ZnO) based thin films deposited by sol-gel spin coating method. J Phys Conf Ser, https://doi.org/10.1088/1742-6596/1116/3/032020
7. Ivanova T, Harizanova A, Koutzarova T, Vertruyen B (2016) Investigation of sol-gel yttrium doped ZnO thin films: structural and optical properties. J Phys Conf Ser 682:012023. https://doi.org/10.1088/1742-6596/682/1/012023.
8. Li L, Yang H, Yang P (2022) Lutetium-doped ZnO to improve photovoltaic performance: a first-principles study. ACS Appl Electron Mater 4(12):6253–6260. https://doi.org/10.1021/acsaelm.2c01365.
9. Parvez MS, Rahman A, Habib AKMA, Nasim Rokon SM (2024) Green synthesis of undoped and yttrium, bismuth co-doped titanium dioxide nanoparticles using Bryophyllum pinnatum for photocatalytic application. Results Mater 24:100629. https://doi.org/10.1016/J.RINMA.2024.100629.
10. Ismail SSM, Ainuddin AR (2019) Effect of annealing temperature on the properties of transition metal doped zinc oxide - a review. In AIP Conference Proceedings, American Institute of Physics Inc. https://doi.org/10.1063/1.5089400.
11. Habibi MH, Sardashti MK (2008) Structure and morphology of nanostructured zinc oxide thin films prepared by dip vs. spin-coating methods. J Iran Chem Soc 5(4):603–609. https://doi.org/10.1007/BF03246140/METRICS.
12. Heo S et al. (2014) Effects of Y contents on surface, structural, optical, and electrical properties for Y-doped ZnO thin films. Thin Solid Films 558:27–30. https://doi.org/10.1016/j.tsf.2014.02.025.
13. Bashir A, Majeed A, Naseem S, Bhatti AS (2021) Investigation of structural and optical parameters of yttrium-doped ZnO thin films

prepared via spin coating of simple aqueous solution. Bull Mater Sci 44(2):95. https://doi.org/10.1007/s12034-021-02391-9.
14. Kaur N, Sharma SK, Kim DY, Singh N (2016) Highly transparent and lower resistivity of yttrium doped ZnO thin films grown on quartz glass by sol–gel method. Phys B Condens Matter 500:179–185. https://doi.org/10.1016/j.physb.2016.08.005.
15. Kaur R, Singh AV, Mehra RM (2006) Sol–gel derived highly transparent and conducting yttrium doped ZnO films. J Non Cryst Solids 352(23–25):2335–2338. https://doi.org/10.1016/j.jnoncrysol.2006.03.011.
16. Kaur N, Sharma SK, Young Kim D (2016) Stress relaxation and transitions in optical bandgap of yttrium doped zinc oxide (YZO) thin films. Curr Appl Phys 16(3):231–239. https://doi.org/10.1016/j.cap.2015.12.004.
17. Bourebia A, Bouaine A, Guendouz H (2024) Appearance of amorphous phase in crystalline In-Y codoped ZnO thin films. Bull Mater Sci 47(2):89. https://doi.org/10.1007/s12034-024-03146-y.
18. Ben Aziza M, Litaiem Y, Chtourou R, Ammar S (2021) The influence of different stabilizers on properties of sol–gel spin-coated zinc oxide films. Braz J Phys 51(3):722–730. https://doi.org/10.1007/s13538-021-00885-9.
19. Ivanova T, Harizanova A, Koutzarova T, Vertruyen B (2017) Sol-gel derived ZnO:Y nanostructured films: structural and optical study. Colloids Surf A Physicochem Eng Asp 532:363–368. https://doi.org/10.1016/j.colsurfa.2017.04.065.
20. Kaur R, Singh AV, Mehra RM (2005) Structural, electrical and optical properties of sol-gel derived yttrium doped ZnO films. Phys Status Solidi Appl Mater Sci 1053–1059. https://doi.org/10.1002/pssa.200420006.
21. Chaitra U, Kekuda D, Mohan Rao K (2017) Effect of annealing temperature on the evolution of structural, microstructural, and optical properties of spin coated ZnO thin films. Ceram Int 43(9):7115–7122. https://doi.org/10.1016/j.ceramint.2017.02.144.
22. Ghanem MG et al. (2019) Synthesis and characterization of undoped and Er-doped ZnO nano-structure thin films deposited by sol-gel spin coating technique. Mater Res Express 6(8):085916. https://doi.org/10.1088/2053-1591/ab2750.
23. Hasabeldaim E, Ntwaeaborwa OM, Kroon RE, Swart HC (2019) Structural, optical and photoluminescence properties of Eu doped ZnO thin films prepared by spin coating. J Mol Struct 1192:105–114. https://doi.org/10.1016/j.molstruc.2019.04.128.
24. Sharma R, Sehrawat K, Wakahara A, Mehra RM (2009) Epitaxial growth of Sc-doped ZnO films on Si by sol–gel route. Appl Surf Sci 255(11):5781–5788. https://doi.org/10.1016/j.apsusc.2009.01.004.
25. Hrytsak L, Turko B, Vasil'ev V, Eliyashevskyy Y, Kostruba A, Hrytsak A (2023) Effect of yttrium doping on the photocatalytic properties of ZnO thin films. Phys Chem Solid State 24(3):422–428. https://doi.org/10.15330/pcss.24.3.422-428.
26. Yu Q et al. (2007) Structural, electrical and optical properties of yttrium-doped ZnO thin films prepared by sol-gel method. J Phys D Appl Phys 40(18):5592–5597. https://doi.org/10.1088/0022-3727/40/18/014.
27. Bazta O et al. (2019) Influence of yttrium doping on the structural, morphological and optical properties of nanostructured ZnO thin films grown by spray pyrolysis. Ceram Int 45(6):6842–6852. https://doi.org/10.1016/j.ceramint.2018.12.178.
28. Ryan AJ, Bras W, Mant GR, Derbyshire GE (1994) A direct method to determine the degree of crystallinity and lamellar thickness of polymers: application to polyethylene. Polymer 35(21):4537–4544. https://doi.org/10.1016/0032-3861(94)90799-4.
29. Rotaru R et al. (2018) Ferromagnetic iron oxide–cellulose nanocomposites prepared by ultrasonication. Polym Chem 9(7):860–868. https://doi.org/10.1039/C7PY01587A.
30. Turko B et al. (2021) Effect of dopant concentration and crystalline structure on the absorption edge in ZnO:Y films. Ukrainian J Phys Opt 22(1):31–37. https://doi.org/10.3116/16091833/22/1/31/2021.
31. Habibi MH, Sardashti MKhaledi (2008) Preparation and proposed mechanism of ZnO nanostructure thin film on glass with highest c-axis orientation. Int J Nanosci Nanotechnol 4(1):13–16.
32. Kumar P, Singh V, Sharma V, Rana G, Malik HK, Asokan K (2015) Investigation of phase segregation in yttrium doped zinc oxide. Ceram Int 41(5):6734–6739. https://doi.org/10.1016/j.ceramint.2015.01.117.
33. Bouaine A, Guendouz H, Schmerber G, Zehouma Y (2019) Synthesis and characterization of Y-doped ZnO thin films prepared by spin-coating technique. Aust J Basic Appl Sci 13(7):49–54. https://doi.org/10.22587/ajbas.2019.13.7.8.
34. Habib AKMA, Rifat KMR, Kabir ME, Khan JN, Rokon SMN, Rabbi MA (2024) Improved photocatalytic activity of (Ni, Mn) co-doped ZnO nanoparticles prepared via green synthesis route using orange peel extract. Results Mater 22, https://doi.org/10.1016/j.rinma.2024.100581.
35. Sharma H, Kumar S, Yadav J, Prasad J, Singh M (2023) Effect of Sn-incorporation on the structural and optical properties of ZnO thin films prepared by sol-gel method. Orient J Chem 39(6):1540–1546. https://doi.org/10.13005/OJC/390614.
36. Sharma SK, Kim DY (2016) Microstructure and optical properties of Yttrium-doped Zinc Oxide (YZO) nanobolts synthesized by hydrothermal method. J Mater Sci Technol 32(1):12–16. https://doi.org/10.1016/J.JMST.2015.11.001.
37. Ahmed S, Sarker MSI, Rahman MM, Kamruzzaman M, Khan MKR (2018) Effect of yttrium(Y) on structural, morphological and transport properties of CdO thin films prepared by spray pyrolysis technique. Heliyon 4(8):e00740. https://doi.org/10.1016/J.HELIYON.2018.E00740.
38. Islam S et al. (2022) Effects of yttrium doping on structural, electrical and optical properties of barium titanate ceramics. Heliyon 8(9):e10529. https://doi.org/10.1016/J.HELIYON.2022.E10529.